# Spinel LiMn$_2$O$_4$ Nanoparticles Grown in Situ on Nitrogen-Doped Reduced Graphene Oxide as an Efficient Cathode for a Li-O$_2$/Li-Ion Twin Battery

Limin Leng,[†,‡] Jing Li,[†] Xiaoyuan Zeng,*[†,§] Huiyu Song,[†] Ting Shu,[†] Haishui Wang,[†] Jianwei Ren,[∥] and Shijun Liao*[†]

[†]The Key Laboratory of Fuel Cell Technology of Guangdong Province, School of Chemistry and Chemical Engineering, South China University of Technology, Guangzhou 510641, China

[‡]Sunwoda Electronic Co., Ltd., Shenzhen, Guangdong 518100, China

[§]Faculty of Metallurgical and Energy Engineering, Kunming University of Science and Technology, Kunming 650093, China

[∥]HySA Infrastructure Centre of Competence, Materials Science and Manufacturing (MSM), Council for Scientific and Industrial Research (CSIR), PO Box 395, Pretoria 0001, South Africa

**S** *Supporting Information*

**ABSTRACT:** Seeking to design high-efficiency catalyst (LMO@N-rGO) for Li-O$_2$ batteries, we suggested a one-step hydrothermal strategy to grow well-crystallized spinel LiMn$_2$O$_4$ (LMO) nanoparticles homogeneously on nitrogen-doped reduced graphene oxide nanosheets (N-rGO). We found that the prepared material can yield a twin-function battery, functioning as a Li-O$_2$ (air) battery under the oxygen atmosphere and a Li-ion battery in the absence of oxygen. In the Li-O$_2$ configuration, the material displayed a lower charge plateau voltage for 0.21 V and excellent cycling performance (120 cycles at 1000 mA h g$^{-1}$ limited capacity). Furthermore, in the absence of oxygen, the material exhibited very good Li-ion battery cathode performance, achieving a capacity of up 80 mA h g$^{-1}$. On the basis of our characterization results, three reasons are suggested for the twin performance of the material: the highly uniform dispersion of LMO nanoparticles, the improved Li diffusion kinetics, and the synergic effect between the spinel LMO nanoparticles and the N-rGO.

**KEYWORDS:** *Nitrogen-doped reduced graphene oxide, Lithium manganese oxide, Oxygen reduction reaction, Li-oxygen battery, Li-ion battery*
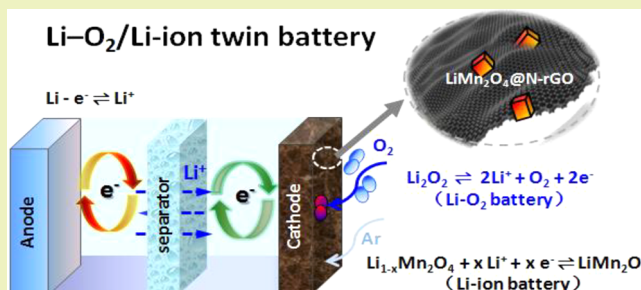
## INTRODUCTION

Considering the ultrahigh theoretical gravimetric energy density (11400 Wh kg$^{-1}$ includes the mass of oxygen and active materials),[1,2] rechargeable Li-O$_2$ batteries have become one of the research hotspots in the field of energy storage. Despite these batteries' huge potential, however, numerous challenges must be addressed before their practical application can be achieved: low round-trip efficiency,[3] inferior cyclability,[4,5] and poor catalytic capability,[6,7] especially at high power density. In a classic nonaqueous Li-O$_2$ configuration, the discharge process involves the oxygen reduction reaction (ORR), yielding insoluble products (such as Li$_2$O$_2$), and for the subsequent oxygen evolution reaction (OER, during recharge process), these discharge products can electrochemical decomposed. In general, advanced cathode materials for the Li-O$_2$ battery usually have an efficient ORR/OER catalyst uniformly distributed on a three-dimensional (3D) porous current collector (Ni/Ti/Cu foam)[8−10] and carbon paper,[11−13] which is beneficial for the deposition and electrochemical decomposition of Li$_2$O$_2$. Therefore, it is desirable to design and synthesize cathode materials with effective catalysts to improve the reversible formation and decomposition of Li$_2$O$_2$.

Recently, spinel oxides have been used in Li-O$_2$ batteries considering their low cost and high efficiency. Spinel oxides consisting of transition metal atoms with multiple valence states, such as CoMn$_2$O$_4$,[14,15] CuCo$_2$O$_4$,[16,17] and NiCo$_2$O$_4$,[18,19] yield promising ORR and OER activity. Spinel LiMn$_2$O$_4$ (which we abbreviate as LMO) has been extensively studied for Li-ion batteries.[20,21] Interestingly, recent studies have revealed $\lambda$-MnO$_2$ to have catalytic activity in water oxidation, the $\lambda$-MnO$_2$ having been derived from spinel LMO following partial Li$^+$ removal.[22] The delithiation of lithium−metal oxides (e.g., LiCoO$_2$[23] or LMO[24,25]) can alter their

electronic structures and enhance their ORR/OER activity in aqueous electrolytes. Chen et al.[26] indicated that the modestly lithiated manganese dioxide ($Li_xMnO_2$, $0 < x < 1$) when acted in a Li-$O_2$ battery as a bifunctional catalyst, the cell showed superior round-trip efficiency and high cyclability. However, the electrocatalytic activity of spinel oxides affected by their poor electronic conductivity. It is urgent that a strategy be developed to enhance the conductivity of the material.

Graphene is not only a good conductive material but also a well-known supporting matrix of metal-based catalyst, so it has been widely used in Li-$O_2$ batteries.[27,28] Nitrogen-doping is a very useful way to modify graphene-based catalysts. Graphene basal planes with added N-doped sites can enhance the ORR activity and further strengthen the electronic conductivity.[29,30] Sun et al.[31] first demonstrated that nitrogen-doped graphene can act in a Li-$O_2$ battery and exhibited a higher discharge capacity compared with undoped graphene nanosheets. In our previous work,[32] we found that the superior ORR performance and high surface area of nitrogen-doped graphene made a great contribution to our high performance PdM/N-rGO (M = Fe, Co, and Ni) materials. So, the nitrogen-doped graphene should be a perfect candidate for promoting the performance of LMO.

On the basis of the above understanding, in this work we developed a composite electrocatalyst (LMO@N-rGO) by the in situ growth of homogeneous LMO nanoparticles on N-rGO via a facile hydrothermal process. Interestingly, this material resulted in a twin Li-$O_2$/Li-ion battery, functioning as a Li-$O_2$ battery under the oxygen atmosphere and a Li-ion battery in the absence of oxygen. For a Li-$O_2$ mode, the hybrid catalyst showed superior ORR and OER activity and yielded high Li-$O_2$ battery performance. In addition, this catalyst also functioned as an outstanding cathode material for a Li-ion battery in the absence of oxygen (its capacity reaching 80 mA h $g^{-1}$), and thus making this a twin Li-$O_2$/Li-ion battery (Figure 1). The high twin performance of our material can attribute to



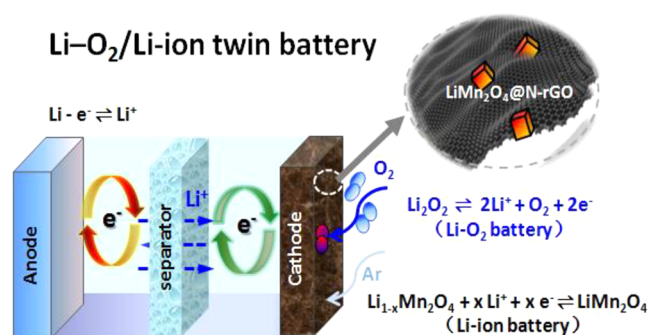**Figure 1.** Schematic of the LMO@N-rGO cathode use as a Li-$O_2$/Li-ion twin battery, showing its functional mechanism.

(i) high dispersion of LMO nanoparticles, assisted by the high surface area of N-rGO; (ii) the improved Li diffusion kinetics achieved by the small particle size of LMO and intimate electrical contact with the porous N-rGO; and (iii) the synergic effect between the N-rGO nanosheets and the spinel LMO nanoparticles.

## EXPERIMENTAL SECTION

**Synthesis of N-rGO Catalyst.** Graphite oxide was prepared as our group reported before.[33] To prepared reduced graphene oxide (rGO) through a thermal treatment process under an argon atmosphere (900 °C for 1 h), nitrogen doping of rGO was synthesized as previously reported.[31] First, the rGO powders were heated at 900 °C (10 °C $min^{-1}$) under an ammonia atmosphere for 2 h. After nitridation, the $NH_3$ gas was immediately switched to $N_2$ gas and the $N_2$ gas flow (50 mL $min^{-1}$) was maintained until the sample had naturally cooled to room temperature for collection.

**Synthesis of LMO@N-rGO Catalyst.** The LMO@N-rGO catalyst was synthesized by a one-step hydrothermal process with some modifications.[34] Specifically, 0.060 g N-rGO powder was added in 60 mL deionized (DI) water by ultrasonic dispersion for 1 h. Next, 2 mL of 1 M $KMnO_4$ solution, 2 mL of 1 M $LiOH \cdot H_2O$, and 3 mL of ethanol were slowly added into this homogeneous suspension, which was then stirred for another 1 h. Then, this mixture was removed to an autoclave to treat at 180 °C for 5 h. To eliminate excessive metal ions and other impurities, these samples were washed with deionized water and ethanol. The reaction product was dried in a freeze-drying machine for 24 h. For comparison, the same process without adding N-rGO was used to prepared pure LMO catalyst. Physical mixtures of pristine N-rGO and LMO (denoted as LMO/N-rGO) cathodes were also prepared via a simple mixing process for comparison purposes.

**Materials Characterization.** Our prepared materials were characterized by FEI's scanning emission electron microscope (Netherlands), JEOL's transmission electron microscope (Japan), Tongda's X-ray powder diffraction (China), HJY's Lab RAM aramis Raman spectrometer (France), and Thermo−VG Scientific's X-ray photoelectron spectroscopy (USA). The distribution of nanoparticles was analyzed using the TEM's Nano Measurer software (version 1.2). Thermal analysis (TA) was carried out on a Q600 SDT instrument (TA Instruments, USA) under air (10 °C $min^{-1}$).

The method to prepare the characterized samples (for SEM/XPS/TEM tests) after discharge/charge process was consistent with our previous report.[32] In order to avoid the moisture and air contamination, an airtight box was used to transfer the samples.

**Electrochemical Testing.** The Li-$O_2$ batteries were prepared as described in our previous publication.[35] The cathode electrode was prepared as follows: the LMO@N-rGO hybrid (80 wt %) was mixed with 20 wt % Nafion solution and stirred for 2 h to form a slurry. For LMO/N-rGO composite electrodes, the slurry contained 80 wt % mixed catalyst (LMO/N-rGO = 75:25 weight ratio) and 20 wt % Nafion solution. The slurry was spread on wet-proof Toray carbon paper and dried in vacuum. The average loading of our material was 0.20 mg $cm^{-2}$. Li-$O_2$ batteries were assembled using a 2032-type coin cell in an Ar-filled glovebox ($H_2O$ < 1.0 ppm, $O_2$ < 1.0 ppm). Lithium metal of 0.35 mm thickness was conducted as the anode, and a Whatman's glass fiber membrane was used as a separator. The electrolyte was 1.0 M $LiN(CF_3SO_2)_2$ in tetraethylene glycol dimethyl ether (TEGDME). Galvanostatic discharge−charge tests were performed on Neware's battery testing system. The specific capacity was normalized based on the total mass of the catalyst unless otherwise specified. Cyclic voltammetry was conducted at Ivium's electrochemical workstation (Netherlands).

## RESULTS AND DISCUSSION

The XRD patterns of various catalysts are shown in Figure 2a. The (001) peak at 10.8° for GO disappeared after heating expansion in argon, while a broad peak at 22.0° emerged, indicating that GO had been successfully prepared. The identical XRD patterns of rGO and N-rGO suggest that the rGO structure remained intact during nitridation. XPS analysis showed the presence of N-doping in the graphene nanosheets, owing to the ammonia reduction of GO (Figure S1, SM). All of the diffraction peaks observed for the LMO@N-rGO sample can be ascribed to the well-crystallized spinel phase (Fd3m, JCPDS 35-0782),[36,37] indicating that no impurities were present. The band observed at 625 $cm^{-1}$ in the Raman spectrum of the LMO@N-rGO sample (Figure S2, SM) is assigned to the LMO spinel phase and can be interpreted as the symmetric Mn−O stretching mode of $MnO_6$ octahedral groups,[38,39] indicating successful synthesis of the LMO@N-
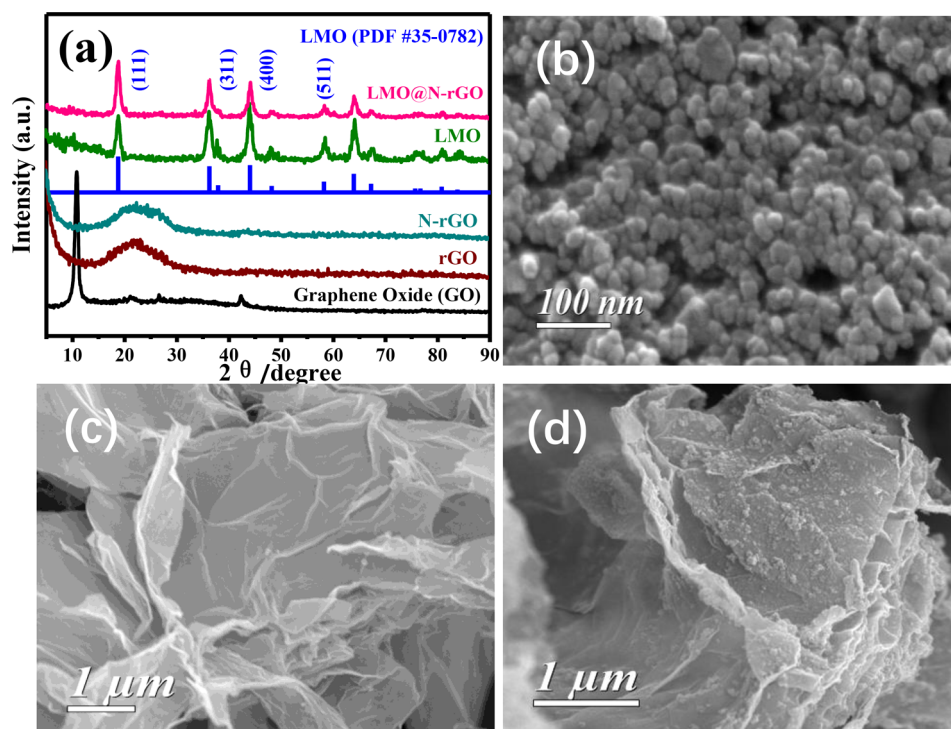
**Figure 2.** (a) XRD patterns of all the as-prepared materials. SEM images of (b) LMO nanoparticles, (c) N-rGO, and (d) LMO@N-rGO.
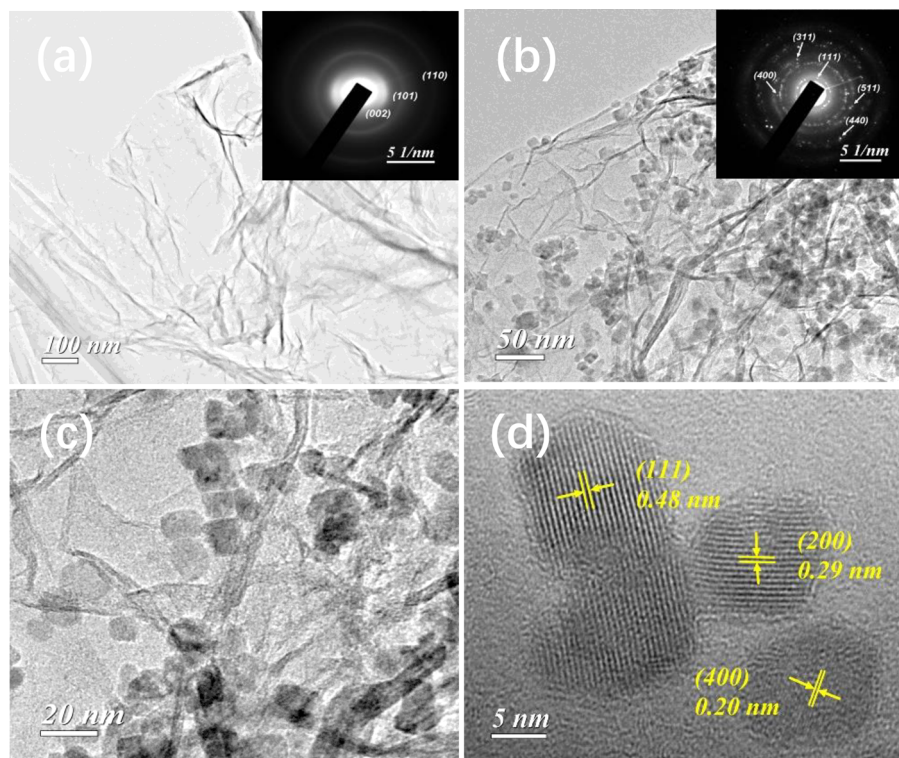


**Figure 3.** TEM images of (a) N-rGO and (b and c) LMO@N-rGO; the insets in (a) and (b) show SAED patterns, (d) HR-TEM image of LMO@N-rGO.

rGO hybrid using the one-step hydrothermal method. As the SEM image in Figure 2d shows, the LMO nanoparticles (see Figure 2b) were well-dispersed on the surface of N-rGO and yielded a coarse surface compared with the pristine morphology of N-rGO (Figure 2c). Additional visual observations obtained by EDS mapping (Figure S3, SM)

demonstrate that manganese and oxygen were homogeneously dispersed on the N-rGO. TG measurement gives an estimated N-rGO content of 25 wt % in the LMO@N-rGO hybrid (Figure S4, SM).

The microstructures of our prepared materials were characterized using TEM and HR-TEM, as shown in Figure
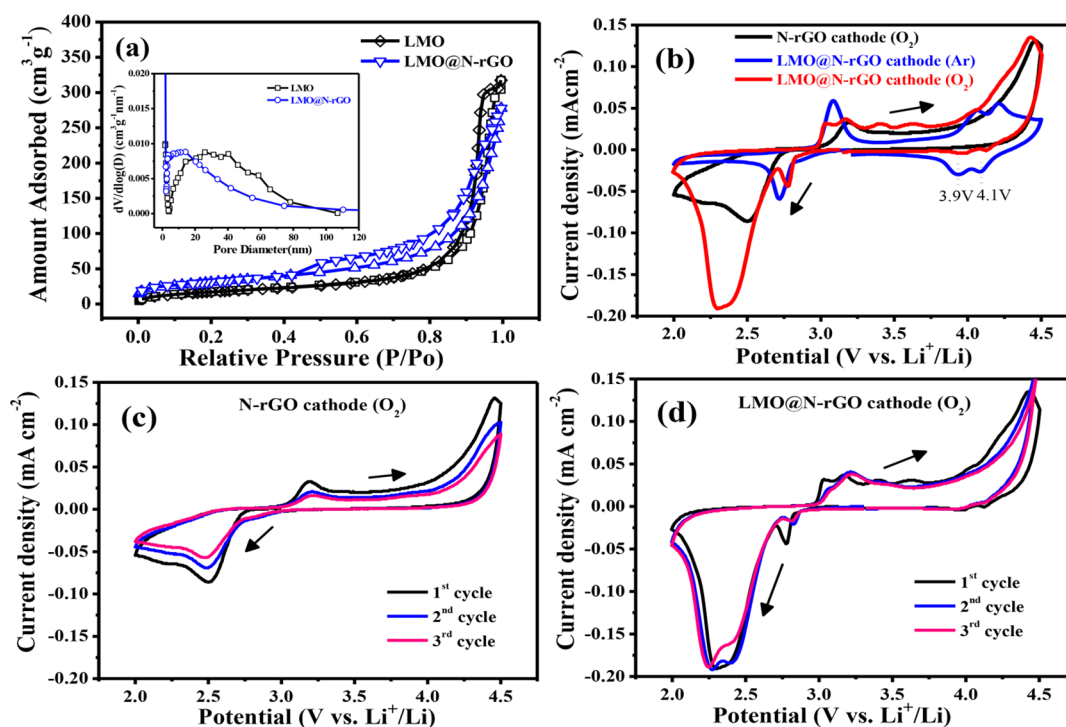
C

**Figure 4.** (a) $N_2$ adsorption−desorption isotherms of LMO and LMO@N-rGO (the inset was the pore-size distributions of these materials); (b, c, and d) cyclic voltammetry curves with different materials at 0.3 mV s$^{-1}$ (2.0−4.5 V).
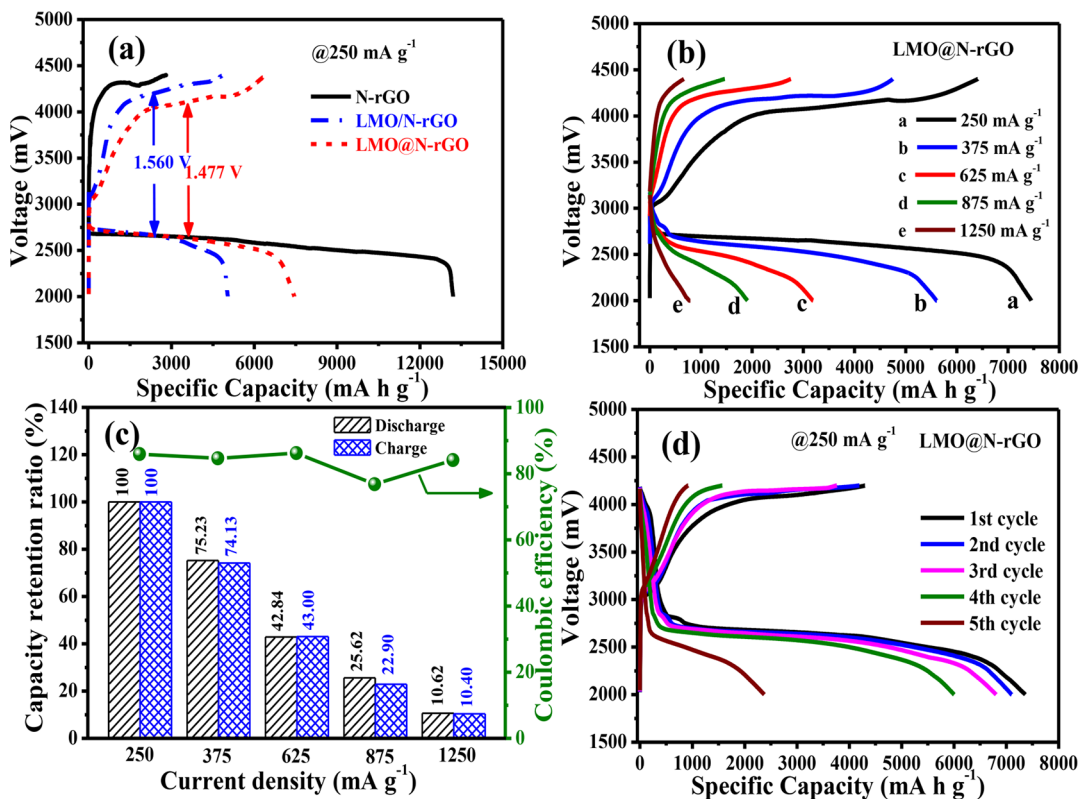


**Figure 5.** (a) Discharge−charge profiles based on different materials at 250 mA g$^{-1}$; (b) with LMO@N-rGO catalyst at different current densities; (c) Coulombic efficiency and capacity retention ratio of Li-$O_2$ cells at different rates with LMO@N-rGO; and (d) cyclic performance of the LMO@N-rGO.

3. LMO nanoparticles (measured by TEM) with a mean particle size of ~9.5 nm (Figure S5, SM) were grown on the porous graphene matrix (Figure 3b and c). The selected area

electron diffraction (SAED) pattern of LMO@N-rGO (inset Figure 3b) reveals several diffraction rings corresponding to LMO (111), (311), (400), (511), and (440), respectively,
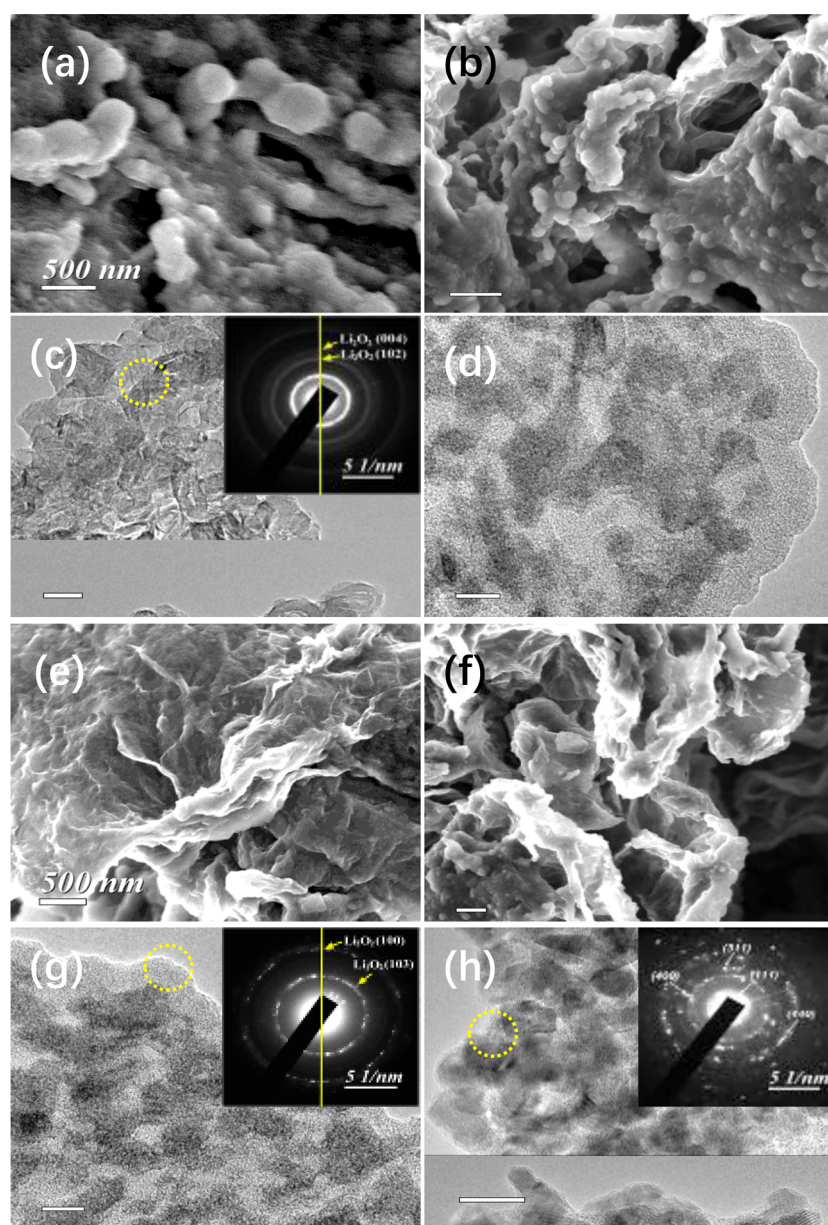
**Figure 6.** SEM and TEM images of the (a, b, c, and d) N-rGO cathode and (e, f, g, and h) LMO@N-rGO cathode after (a, c, e, and g) first full discharge (to 2.0 V) and (b, d, f, and h) following recharge (to 4.4 V) (insets show SAED patterns).

which are consistent with the XRD results. The measured interplanar spacing values of 0.48, 0.29, and 0.20 nm from the HR-TEM image shown in Figure 3d correspond to the (111), (200), and (400) planes of LMO, respectively.

The pore structures of the LMO and LMO@N-rGO hybrid catalysts were characterized using $N_2$ adsorption−desorption isotherms (Figure 4a). The BET surface areas of the LMO and LMO@N-rGO samples are calculated to 63.7 and 108.5 $m^2$ $g^{-1}$, respectively. The corresponding PSDs of the catalysts determined by BJH branch based on the BJH method (inset Figure 4a) shows that LMO@N-rGO has a higher pore density than LMO in the 2−20 nm range, which is attributable to the structure of N-rGO (542.6 $m^2$ $g^{-1}$, Figure S6, SM).

To study the ORR and OER activity of the synthesized catalysts in an aprotic electrolyte, the CV method was conducted as Figure 4b shown. It can be seen that in an $O_2$ atmosphere, LMO@N-rGO (Figure 4d) exhibited enhanced ORR and OER activity and stability compared to N-rGO

(Figure 4c), which confirms the merits of the composite catalyst. In an argon atmosphere, nearly no ORR was observed for LMO@N-rGO, other than a very small peak, which may have been related to residual oxygen. However, the OER performance of LMO@N-rGO was quite different, with redox potentials between 2.70 and 3.2 V, which corresponds to the occurrence of a two-phase transfer reaction involving cubic LMO and tetragonal $Li_2Mn_2O_4$.[37,40−42] The cubic-to-tetragonal transition is due to the Jahn−Teller distortion associated with the single electron in the e orbital of $Mn^{3+}$ ions as the average oxidation state of Mn falls below 3.5. However, the peaks with Li-ion intercalation and extraction reaction could not be found between 3.8 and 4.2 V. We suggest the main reason is that the Li-ion intercalation is a parallel reaction with decomposition of $Li_2O_2$ between 3.8 to 4.2 V, thus the intercalation reaction is severely suppressed by the decomposition reaction. Interestingly, in an argon atmosphere, the LMO@N-rGO exhibited a clear peak between 3.8 and 4.2 V,
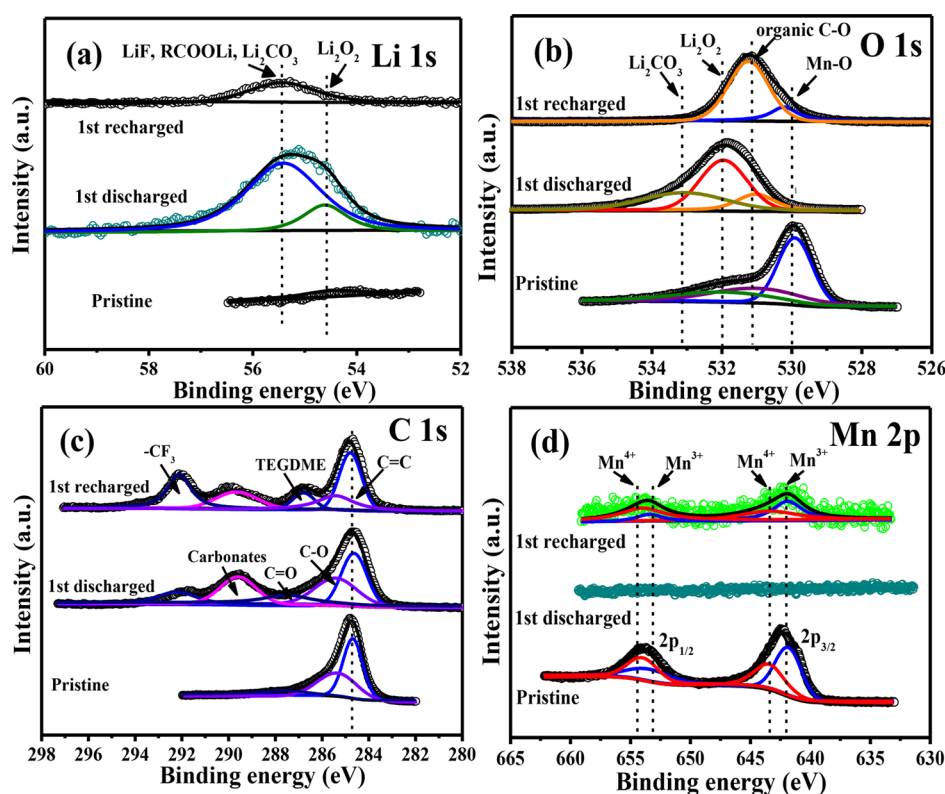
**Figure 7.** XPS spectra of (a) Li 1s, (b) O 1s, (c) C 1s, and (d) Mn 2p core peaks of the LMO@N-rGO electrode after first discharge to 2.0 V and following recharge to 4.4 V.

corresponding to Li-ion intercalation and extraction.[43,44] In other words, the LMO@N-rGO cathode material was able to act not only for a Li-O$_2$ cell but also for a Li-ion battery.[45] Once oxygen/air is supplied, the battery is a Li-O$_2$ battery; if no oxygen/air is supplied, it is a Li-ion battery. This characteristic makes the battery convertible between the two types of batteries.

Figure 5a compares the first galvanostatic discharge—charge profiles of Li-O$_2$ cells with our prepared cathode catalysts. Li-O$_2$ batteries with LMO/N-rGO and LMO@N-rGO materials achieved specific discharge capacities of 5041.2 and 7455 mA h g$^{-1}$, respectively, with similar discharge plateaus of approximately 2.70 V versus Li/Li$^+$, which were larger than some metal oxide cathode catalysts reported previously.[46,47] It should be noted that the capacity of the N-rGO cathode reached 13206.2 mA h g$^{-1}$, which may have been due to the high surface area and good ORR performance brought about by nitrogen-doping and the abundance of macropores, consistent with that previously reported by our group.[32] Although those factors may have been beneficial for the deposition of discharge products, this battery had the highest recharge plateau potential, at approximately 4.305 V, which is in agreement with previous reports.[48,49] In addition, the battery with a N-rGO cathode exhibited poor stability, as we will discuss later.

We also measured the battery's performance in an argon atmosphere; interestingly, the battery's capacity reached 80 mA h g$^{-1}$ (Figure S7, SM). Obviously, this capacity should be attributed to the Li-ion battery behavior of the material, indicating that LMO/N-rGO material can function in both Li-O$_2$ and Li-ion batteries, although its Li-ion capacity is much lower than its Li-O$_2$ capacity. The above analysis allows us to

conclude that the significantly enhanced discharge capacity of the Li-O$_2$ battery with LMO@N-rGO material should derive from the material's oxygen reduction ability but not its Li-ion behavior.

Notably, the LMO@N-rGO (or LMO/N-rGO) cathode battery showed a lower charge plateau potential than the N-rGO battery, indicating the former's large Coulombic efficiency for reversible reactions. What caused such high efficiency? We propose three possible factors: (i) the catalysis of LMO toward the ORR and OER, especially the OER; (ii) possible lithium extraction from LMO, which tunes its electronic properties, surface structure, and oxidation state, making the decomposition of Li$_2$O$_2$ easy;[26,50] and (iii) the synergetic interaction of N-rGO and LMO. Importantly, the LMO@N-rGO cathode also exhibited high charge—discharge rate capability. Under the current densities of 375, 625, and 875 mA g$^{-1}$, the discharge capacities reached 5608, 3193, and 1910 mA h g$^{-1}$, respectively (Figure 5b), corresponding to capacity retention ratios of 75.2%, 43.0%, and 22.9% (Figure 5c). The battery preserves nearly 80% Coulombic efficiency (the ratio of charge capacity to discharge capacity) at all the investigated rates.

We also investigated the stability of the batteries with various cathodes. The LMO@N-rGO-based Li-O$_2$ battery had a capacity retention of up to 93.7%, with a preserved capacity of 6005 mA h g$^{-1}$ after four cycles (Figure 5d). In contrast, the capacities of the batteries with N-rGO or LMO/N-rGO as the cathode decayed rapidly; after four cycles the capacity was less than 20% (Figure S8, SM). This may have been due to the continuous rise in resistance resulting from the formation of poor reversible Li$_2$O$_2$ on the cathodes.

To further explore the reversibility of the various cathodes, we disassembled the batteries with the prepared cathodes in
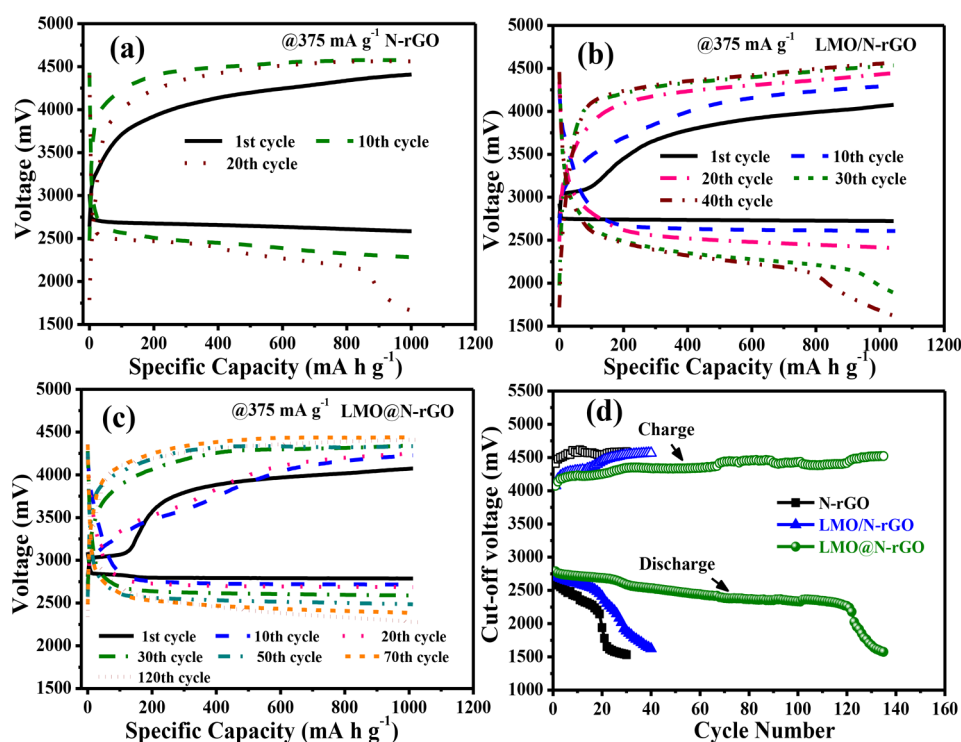
**Figure 8.** Cyclic performance of Li-O$_2$ batteries with (a) N-rGO, (b) LMO/N-rGO, and (c) LMO@N-rGO catalysts at 375 mA g$^{-1}$ with a curtailing capacity of 1000 mA h g$^{-1}$; and (d) the terminal voltages as a functional of cycle number.

their discharged and charged states. The different charged and discharged states of the N-rGO cathodes and LMO@N-rGO cathodes were characterized by SEM and TEM shown in Figure 6. After discharge, the pores inside the N-rGO electrode were partially filled with insoluble reduction products that exhibited a spherical, closed morphology (Figure 6a). The TEM image in Figure 6c shows a homogeneous coating on the discharge products that was identified as Li$_2$O$_2$ (see the inset SAED pattern). After recharge, some small discharge products still randomly remained on the N-rGO electrode (Figure 6b), suggesting the poor reversibility of Li$_2$O$_2$ with the N-rGO electrode. Indeed, residual deposition of insoluble Li$_2$O$_2$ on the N-rGO cathode reduced electronic conductivity and oxygen diffusion, leading to an increase in the cathode's polarization and the battery's subsequent rapid decay. The result was quite different with LMO@N-rGO as the cathode. After discharge, a curly morphology and a smooth surface was obtained (Figure 6e), and SAED confirmed that the thin layer uniformly covering the cathode's surface was Li$_2$O$_2$ (inset Figure 6g). We found that the discharge products on the surface of the LMO/N-rGO and LMO@N-rGO cathodes could be decomposed during the subsequent charge process, leaving numerous bumps on the LMO/N-rGO (Figure S9b, SM) and LMO@N-rGO electrodes (Figure 6d). Clearly, the formation/decomposition of Li$_2$O$_2$ on the LMO@N-rGO cathode is a reversible process, which contributes to the better stability of the LMO@N-rGO electrode compared to the N-rGO electrode. SAED (inset Figure 6h) confirmed that the surface bumps of the recharged LMO@N-rGO electrode were Li$_{1-x}$Mn$_2$O$_4$ nanoparticles ($0 < x < 1$). On the one hand, the well-dispersed LMO nanoparticles on N-rGO increased the utilization of the active species and facilitated the uniform distribution of discharge products. On the other hand, the delithiation of LMO nanoparticles altered their electronic

structures and reduced the migration path length of lithium ions, which may have promoted the decomposition of Li$_2$O$_2$ on charging. With this in mind, we conducted XPS analysis to confirm the reversibility of Li$_2$O$_2$ in the first cycle as shown in Figure 7. The Li 1s region of the discharged cathode included contributions from the underlying Li$_2$O$_2$ and surface lithium carbonate species (Figure 7a) due to the electrolyte decomposition, as reported previously by other groups.[51,52] After charging, the Li 1s peaks corresponding to Li$_2$O$_2$ disappeared, revealing the existence of surface carbonate species. Meanwhile, the disappearance of the Mn 2p peak (Figure 7d) indicates that all LMO particles were covered by discharge products, which is consistent with the SEM image (Figure 6c). Insoluble products such as Li$_2$O$_2$ and inorganic Li$_2$CO$_3$ can precipitate as byproducts of parasitic reactions resulting from TEGDME decomposition[53,54] and carbon material corrosion during discharge, as reported previously.[55] The reappearance of the Mn 2p peak when the batteries were charged to 4.4 V shows that the electrochemical reaction was somewhat reversible.

To further clarify the better cyclability of the LMO@N-rGO-based Li-O$_2$ battery, the cell was cycled at 375 mA g$^{-1}$ in the limited capacity of 1000 mA h g$^{-1}$ (Figure 8). As expected, the battery's potential gradually decayed within 122 cycles (Figure 8c), and no sudden decay was observed, unlike some metal oxide catalysts (which have high capacity but poor cycling stability).[56-58] In contrast, in the batteries with N-rGO or LMO/N-rGO as the cathodes, sudden decay occurred in the 18th cycles and 28th cycles, respectively (Figure 7d). Further, compared with previously reported spinel metal oxide-based catalysts (Table S1),[59,60] the LMO@N-rGO cathode also exhibited much better stability/reversibility.

To test the Li-ion performance of the battery containing the LMO@N-rGO cathode, we investigated its charge–discharge

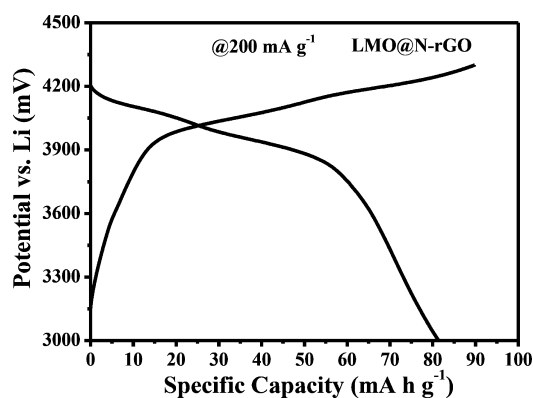behavior in an argon atmosphere (Figure 9). The initial capacity of the LMO@N-rGO nanocomposite electrode was



**Figure 9.** First-cycle voltage profiles of LMO@N-rGO between 3.0 and 4.3 V at 200 mA g$^{-1}$.

81.37 mA h g$^{-1}$, and the Coulombic efficiency was about 91%. This confirmed that it functions for a Li-O$_2$ battery and for a Li-ion battery, giving it twin functionality.

## CONCLUSION

In summary, we have successfully prepared a novel cathode material via a simple one-step hydrothermal method by growing spinel LMO nanoparticles uniformly on N-rGO nanosheets. It is first found that a battery with LMO@N-rGO cathode can function as a twin battery: Li-O$_2$ battery (with O$_2$) and Li-ion battery (without O$_2$). The Li-O$_2$ cell with LMO@N-rGO cathode exhibited high capacity (7455 mAh g$^{-1}$ at 250 mA g$^{-1}$) and excellent stability (120 cycles) at a limited capacity of 1000 mAh g$^{-1}$. To act as a Li-ion battery, the LMO@N-rGO electrode delivered a capacity of up to 80 mAh g$^{-1}$. This work for the first time raises the possibility of using LMO@N-rGO as a highly effective, low-cost cathode for rechargeable Li-O$_2$ battery, Li-ion battery, and possibly Li-O$_2$/Li-ion twin batteries, making a useful new type of battery possible and used for certain specialized applications.

## ASSOCIATED CONTENT

**Ⓢ Supporting Information**

The Supporting Information is available free of charge on the ACS Publications website at DOI: 10.1021/acssusche-meng.8b03849.

> XPS survey spectra, the N 1s spectra, Raman spectra, elemental mapping, TGA curves, particle size distribution, N$_2$ adsorption−desorption isotherms, the pore size distributions, the discharge−charge curves of Li-O$_2$ batteries in Ar atmosphere and O$_2$ atmosphere, SEM images after discharge and recharge, and the comparison of battery performance of Li-O$_2$ batteries (PDF)

## AUTHOR INFORMATION

**Corresponding Authors**
*E-mail: zengxiaoyuan721@126.com.
*E-mail: chsjliao@scut.edu.cn.
**ORCID** Ⓞ
Xiaoyuan Zeng: 0000-0001-8596-1094
Shijun Liao: 0000-0003-2481-0377

**Notes**
The authors declare no competing financial interest.

## REFERENCES

(1) Bruce, P. G.; Freunberger, S. A.; Hardwick, L. J.; Tarascon, J.-M. Li-O$_2$ and Li-S batteries with high energy storage. *Nat. Mater.* **2012**, *11* (1), 19−29.

(2) Li, Y.; Wang, X.; Dong, S.; Chen, X.; Cui, G. Recent Advances in Non-Aqueous Electrolyte for Rechargeable Li-O$_2$ Batteries. *Adv. Energy Mater.* **2016**, *6* (18), 1600751.

(3) Lu, J.; Li, L.; Park, J.-B.; Sun, Y.-K.; Wu, F.; Amine, K. Aprotic and Aqueous Li-O$_2$ Batteries. *Chem. Rev.* **2014**, *114* (11), 5611−5640.

(4) Ryan, K. R.; Trahey, L.; Ingram, B. J.; Burrell, A. K. Limited Stability of Ether-Based Solvents in Lithium-Oxygen Batteries. *J. Phys. Chem. C* **2012**, *116* (37), 19724−19728.

(5) Itkis, D. M.; Semenenko, D. A.; Kataev, E. Y.; Belova, A. I.; Neudachina, V. S.; Sirotina, A. P.; Havecker, M.; Teschner, D.; Knop-Gericke, A.; Dudin, P.; Barinov, A.; Goodilin, E. A.; Shao-Horn, Y.; Yashina, L. V. Reactivity of Carbon in Lithium-Oxygen Battery Positive Electrodes. *Nano Lett.* **2013**, *13* (10), 4697−4701.

(6) Mirzaeian, M.; Hall, P. J.; Sillars, F. B.; Fletcher, I.; Goldin, M. M.; Shitta-bey, G. O.; Jirandehi, H. F. The Effect of Operation Conditions on the Performance of Lithium/Oxygen Batteries. *J. Electrochem. Soc.* **2013**, *160* (1), A25−A30.

(7) Nemanick, E. J.; Hickey, R. P. The effects of O$_2$ pressure on Li-O$_2$ secondary battery discharge capacity and rate capability. *J. Power Sources* **2014**, *252*, 248−251.

(8) Zhao, G.; Mo, R.; Wang, B.; Zhang, L.; Sun, K. Enhanced Cyclability of Li-O$_2$ Batteries Based on TiO$_2$ Supported Cathodes with No Carbon or Binder. *Chem. Mater.* **2014**, *26* (8), 2551−2556.

(9) Tian, X. L.; Xu, Y. Y.; Zhang, W.; Wu, T.; Xia, B. Y.; Wang, X. Unsupported Platinum-Based Electrocatalysts for Oxygen Reduction Reaction. *Acs Energy Letters* **2017**, *2* (9), 2035−2043.

(10) Leng, L.; Zeng, X.; Song, H.; Shu, T.; Wang, H.; Liao, S. Pd nanoparticles decorating flower-like Co$_3$O$_4$ nanowire clusters to form an efficient, carbon/binder-free cathode for Li-O$_2$ batteries. *J. Mater. Chem. A* **2015**, *3* (30), 15626−15632.

(11) Kim, Y.; Park, J. H.; Kim, J. G.; Noh, Y.; Kim, Y.; Han, H.; Kim, W. B. Ruthenium Oxide Incorporated One-Dimensional Cobalt Oxide Composite Nanowires as Lithium−Oxygen Battery Cathode Catalysts. *ChemCatChem* **2017**, *9* (18), 3554−3562.

(12) Zhang, Y.; Li, X.; Zhang, M.; Liao, S.; Dong, P.; Xiao, J.; Zhang, Y.; Zeng, X. IrO$_2$ nanoparticles highly dispersed on nitrogen-doped carbon nanotubes as an efficient cathode catalyst for high-performance Li-O$_2$ batteries. *Ceram. Int.* **2017**, *43* (16), 14082−14089.

(13) Liu, Q.-c.; Xu, J.-j.; Chang, Z.-w.; Zhang, X.-b. Direct electrodeposition of cobalt oxide nanosheets on carbon paper as free-standing cathode for Li-O$_2$ battery. *J. Mater. Chem. A* **2014**, *2* (17), 6081−6085.

(14) Wang, L.; Zhao, X.; Lu, Y.; Xu, M.; Zhang, D.; Ruoff, R. S.; Stevenson, K. J.; Goodenough, J. B. CoMn$_2$O$_4$ Spinel Nanoparticles Grown on Graphene as Bifunctional Catalyst for Lithium-Air Batteries. *J. Electrochem. Soc.* **2011**, *158* (12), A1379.

(15) Zhai, X.; Yang, W.; Li, M.; Lv, G.; Liu, J.; Zhang, X. Noncovalent hybrid of CoMn$_2$O$_4$ spinel nanocrystals and poly (diallyldimethylammonium chloride) functionalized carbon nano-

tubes as efficient electrocatalysts for oxygen reduction reaction. *Carbon* **2013**, *65*, 277–286.

(16) Serov, A.; Andersen, N. I.; Roy, A. J.; Matanovic, I.; Artyushkova, K.; Atanassov, P. CuCo$_2$O$_4$ ORR/OER Bi-Functional Catalyst: Influence of Synthetic Approach on Performance. *J. Electrochem. Soc.* **2015**, *162* (4), F449–F454.

(17) Liu, Y.; Cao, L.-J.; Cao, C.-W.; Wang, M.; Leung, K.-L.; Zeng, S.-S.; Hung, T. F.; Chung, C. Y.; Lu, Z.-G. Facile synthesis of spinel CuCo$_2$O$_4$ nanocrystals as high-performance cathode catalysts for rechargeable Li−air batteries. *Chem. Commun.* **2014**, *50* (93), 14635–14638.

(18) Peng, S.; Hu, Y.; Li, L.; Han, X.; Cheng, F.; Srinivasan, M.; Yan, Q.; Ramakrishna, S.; Chen, J. Controlled synthesis of porous spinel cobaltite core-shell microspheres as high-performance catalysts for rechargeable Li-O$_2$ batteries. *Nano Energy* **2015**, *13*, 718–726.

(19) Sun, B.; Huang, X.; Chen, S.; Zhao, Y.; Zhang, J.; Munroe, P.; Wang, G. Hierarchical macroporous/mesoporous NiCo$_2$O$_4$ nanosheets as cathode catalysts for rechargeable Li-O$_2$ batteries. *J. Mater. Chem. A* **2014**, *2* (30), 12053–12059.

(20) Kim, D. K.; Muralidharan, P.; Lee, H.-W.; Ruffo, R.; Yang, Y.; Chan, C. K.; Peng, H.; Huggins, R. A.; Cui, Y. Spinel LiMn$_2$O$_4$ Nanorods as Lithium Ion Battery Cathodes. *Nano Lett.* **2008**, *8* (11), 3948–3952.

(21) Lee, H.-W.; Muralidharan, P.; Ruffo, R.; Mari, C. M.; Cui, Y.; Kim, D. K. Ultrathin Spinel LiMn$_2$O$_4$ Nanowires as High Power Cathode Materials for Li-Ion Batteries. *Nano Lett.* **2010**, *10* (10), 3852–3856.

(22) Robinson, D. M.; Go, Y. B.; Greenblatt, M.; Dismukes, G. C. Water Oxidation by $\lambda$-MnO$_2$: Catalysis by the Cubical Mn$_4$O$_4$ Subcluster Obtained by Delithiation of Spinel LiMn$_2$O$_4$. *J. Am. Chem. Soc.* **2010**, *132* (33), 11467–11469.

(23) Maiyalagan, T.; Jarvis, K. A.; Therese, S.; Ferreira, P. J.; Manthiram, A. Spinel-type lithium cobalt oxide as a bifunctional electrocatalyst for the oxygen evolution and oxygen reduction reactions. *Nat. Commun.* **2014**, *5*, 3949.

(24) Liu, Y.; Li, J.; Li, W.; Li, Y.; Chen, Q.; Liu, Y. Spinel LiMn$_2$O$_4$ nanoparticles dispersed on nitrogen-doped reduced graphene oxide nanosheets as an efficient electrocatalyst for aluminium-air battery. *Int. J. Hydrogen Energy* **2015**, *40* (30), 9225–9234.

(25) Park, J.; Kim, H.; Jin, K.; Lee, B. J.; Park, Y.-S.; Kim, H.; Park, I.; Yang, K. D.; Jeong, H.-Y.; Kim, J.; Hong, K. T.; Jang, H. W.; Kang, K.; Nam, K. T. A New Water Oxidation Catalyst: Lithium Manganese Pyrophosphate with Tunable Mn Valency. *J. Am. Chem. Soc.* **2014**, *136* (11), 4201–4211.

(26) Hu, Y.; Zhang, T.; Cheng, F.; Zhao, Q.; Han, X.; Chen, J. Recycling Application of Li−MnO$_2$ Batteries as Rechargeable Lithium−Air Batteries. *Angew. Chem., Int. Ed.* **2015**, *54* (14), 4338–4343.

(27) Kim, J. G.; Kim, Y.; Noh, Y.; Lee, S.; Kim, Y.; Kim, W. B. Bifunctional Hybrid Catalysts with Perovskite LaCo$_{0.8}$Fe$_{0.2}$O$_3$ Nanowires and Reduced Graphene Oxide Sheets for an Efficient Li-O$_2$ Battery Cathode. *ACS Appl. Mater. Interfaces* **2018**, *10* (6), 5429–5439.

(28) Storm, M. M.; Overgaard, M.; Younesi, R.; Reeler, N. E. A.; Vosch, T.; Nielsen, U. G.; Edström, K.; Norby, P. Reduced graphene oxide for Li−air batteries: The effect of oxidation time and reduction conditions for graphene oxide. *Carbon* **2015**, *85*, 233–244.

(29) Yang, H. B.; Miao, J.; Hung, S.-F.; Chen, J.; Tao, H. B.; Wang, X.; Zhang, L.; Chen, R.; Gao, J.; Chen, H. M.; et al. Identification of catalytic sites for oxygen reduction and oxygen evolution in N-doped graphene materials: Development of highly efficient metal-free bifunctional electrocatalyst. *Science advances* **2016**, *2* (4), No. e1501122.

(30) Nazarian-Samani, M.; Lim, H.-D.; Haghighat-Shishavan, S.; Kim, H.-K.; Ko, Y.; Kim, M.-S.; Lee, S.-W.; Kashani-Bozorg, S. F.; Abbasi, M.; Guim, H.-U.; et al. A robust design of Ru quantum dot/N-doped holey graphene for efficient Li-O$_2$ batteries. *J. Mater. Chem. A* **2017**, *5* (2), 619–631.

(31) Li, Y. L.; Wang, J. J.; Li, X. F.; Geng, D. S.; Banis, M. N.; Li, R. Y.; Sun, X. L. Nitrogen-doped graphene nanosheets as cathode materials with excellent electrocatalytic activity for high capacity lithium-oxygen batteries. *Electrochem. Commun.* **2012**, *18*, 12–15.

(32) Leng, L.; Li, J.; Zeng, X.; Song, H.; Shu, T.; Wang, H.; Liao, S. Enhancing the cyclability of Li-O$_2$ batteries using PdM alloy nanoparticles anchored on nitrogen-doped reduced graphene as the cathode catalyst. *J. Power Sources* **2017**, *337*, 173–179.

(33) Qiao, X.; You, C.; Shu, T.; Fu, Z.; Zheng, R.; Zeng, X.; Li, X.; Liao, S. A one-pot method to synthesize high performance multielement co-doped reduced graphene oxide catalysts for oxygen reduction. *Electrochem. Commun.* **2014**, *47*, 49–53.

(34) Jo, K.-Y.; Han, S.-Y.; Lee, J. M.; Kim, I. Y.; Nahm, S.; Choi, J.-W.; Hwang, S.-J. Remarkable enhancement of the electrode performance of nanocrystalline LiMn$_2$O$_4$ via solvothermally-assisted immobilization on reduced graphene oxide nanosheets. *Electrochim. Acta* **2013**, *92*, 188–196.

(35) Zeng, X.; Dang, D.; Leng, L.; You, C.; Wang, G.; Zhu, C.; Liao, S. Doped reduced graphene oxide mounted with IrO$_2$ nanoparticles shows significantly enhanced performance as a cathode catalyst for Li-O$_2$ batteries. *Electrochim. Acta* **2016**, *192*, 431–438.

(36) Gummow, R. J.; Thackeray, M. M. An Investigation of Spinel-Related and Orthorhombic LiMnO$_2$ Cathodes for Rechargeable Lithium Batteries. *J. Electrochem. Soc.* **1994**, *141* (5), 1178–1182.

(37) Liu, W.; Kowal, K.; Farrington, G. C. Mechanism of the Electrochemical Insertion of Lithium into LiMn$_2$O$_4$ Spinels. *J. Electrochem. Soc.* **1998**, *145* (2), 459–465.

(38) Ramana, C. V.; Massot, M.; Julien, C. M. XPS and Raman spectroscopic characterization of LiMn$_2$O$_4$ spinels. *Surf. Interface Anal.* **2005**, *37* (4), 412–416.

(39) Pröll, J.; Kohler, R.; Torge, M.; Ulrich, S.; Ziebert, C.; Bruns, M.; Seifert, H. J.; Pfleging, W. Laser microstructuring and annealing processes for lithium manganese oxide cathodes. *Appl. Surf. Sci.* **2011**, *257* (23), 9968–9976.

(40) Kang, S. H.; Goodenough, J. B. Li [ Mn$_2$ ] O$_4$ Spinel Cathode Material Showing No Capacity Fading in the 3 V Range. *J. Electrochem. Soc.* **2000**, *147* (10), 3621–3627.

(41) Sakaushi, K.; Fellinger, T.-P.; Antonietti, M. Bifunctional Metal-Free Catalysis of Mesoporous Noble Carbons for Oxygen Reduction and Evolution Reactions. *ChemSusChem* **2015**, *8* (7), 1156–1160.

(42) Park, J.; Jeong, J.; Lee, S.; Jo, C.; Lee, J. Effect of Mesoporous Structured Cathode Materials on Charging Potentials and Rate Capability of Lithium−Oxygen Batteries. *ChemSusChem* **2015**, *8* (18), 3146–3152.

(43) Tarascon, J. M.; Wang, E.; Shokoohi, F. K.; McKinnon, W. R.; Colson, S. The Spinel Phase of LiMn2 O 4 as a Cathode in Secondary Lithium Cells. *J. Electrochem. Soc.* **1991**, *138* (10), 2859–2864.

(44) Li, F.; Ohnishi, R.; Yamada, Y.; Kubota, J.; Domen, K.; Yamada, A.; Zhou, H. Carbon supported TiN nanoparticles: an efficient bifunctional catalyst for non-aqueous Li-O$_2$ batteries. *Chem. Commun.* **2013**, *49* (12), 1175–1177.

(45) Wang, D.; Shen, Y.; Hong, K.; Huang, Q.; Huang, Y. A high-capacity Li-ion/Li−oxygen hybrid cathode. *J. Mater. Chem. A* **2015**, *3* (26), 13628–13631.

(46) Zhang, X.; Zhang, X.; Wang, X.-G.; Xie, Z.; Zhou, Z. NiFe$_2$O$_4$−CNT composite: an efficient electrocatalyst for oxygen evolution reactions in Li-O$_2$ batteries guided by computations. *J. Mater. Chem. A* **2016**, *4* (24), 9390–9393.

(47) Cao, X.; Sun, Z.; Zheng, X.; Tian, J.; Jin, C.; Yang, R.; Li, F.; He, P.; Zhou, H. MnCo$_2$O$_4$ decorated Magnéli phase titanium oxide as a carbon-free cathode for Li-O$_2$ batteries. *J. Mater. Chem. A* **2017**, *5* (37), 19991–19996.

(48) Dong, S.; Chen, X.; Zhang, K.; Gu, L.; Zhang, L.; Zhou, X.; Li, L.; Liu, Z.; Han, P.; Xu, H.; Yao, J.; Zhang, C.; Zhang, X.; Shang, C.; Cui, G.; Chen, L. Molybdenum nitride based hybrid cathode for rechargeable lithium-O$_2$ batteries. *Chem. Commun.* **2011**, *47* (40), 11291–11293.

(49) Guo, X.; Liu, P.; Han, J.; Ito, Y.; Hirata, A.; Fujita, T.; Chen, M. 3D Nanoporous Nitrogen-Doped Graphene with Encapsulated RuO2

Nanoparticles for Li-O$_2$ Batteries. *Adv. Mater.* **2015**, *27* (40), 6137–6143.

(50) Lee, J.-H.; Black, R.; Popov, G.; Pomerantseva, E.; Nan, F.; Botton, G. A.; Nazar, L. F. The role of vacancies and defects in Na$_{0.44}$MnO$_2$ nanowire catalysts for lithium–oxygen batteries. *Energy Environ. Sci.* **2012**, *5* (11), 9558–9565.

(51) Kundu, D.; Black, R.; Berg, E. J.; Nazar, L. F. A highly active nanostructured metallic oxide cathode for aprotic Li-O$_2$ batteries. *Energy Environ. Sci.* **2015**, *8* (4), 1292–1298.

(52) Lu, Y.; Ang, H.; Yan, Q.; Fong, E. Bioinspired Synthesis of Hierarchically Porous MoO$_2$/Mo$_2$C Nanocrystal Decorated N-Doped Carbon Foam for Lithium–Oxygen Batteries. *Chem. Mater.* **2016**, *28* (16), 5743–5752.

(53) Carboni, M.; Brutti, S.; Marrani, A. G. Surface Reactivity of a Carbonaceous Cathode in a Lithium Triflate/Ether Electrolyte-Based Li-O$_2$ Cell. *ACS Appl. Mater. Interfaces* **2015**, *7* (39), 21751–21762.

(54) Freunberger, S. A.; Chen, Y.; Drewett, N. E.; Hardwick, L. J.; Bardé, F.; Bruce, P. G. The Lithium–Oxygen Battery with Ether-Based Electrolytes. *Angew. Chem., Int. Ed.* **2011**, *50* (37), 8609–8613.

(55) Lu, J.; Lei, Y.; Lau, K. C.; Luo, X.; Du, P.; Wen, J.; Assary, R. S.; Das, U.; Miller, D. J.; Elam, J. W.; Albishri, H. M.; El-Hady, D. A.; Sun, Y.-K.; Curtiss, L. A.; Amine, K. A nanostructured cathode architecture for low charge overpotential in lithium-oxygen batteries. *Nat. Commun.* **2013**, *4*, 2383.

(56) Li, P.; Sun, W.; Yu, Q.; Yang, P.; Qiao, J.; Wang, Z.; Rooney, D.; Sun, K. An effective three-dimensional ordered mesoporous CuCo$_2$O$_4$ as electrocatalyst for Li-O$_2$ batteries. *Solid State Ionics* **2016**, *289*, 17–22.

(57) Wang, J.; Liu, L.; Subramaniyam, C. M.; Chou, S.; Liu, H.; Wang, J. A microwave autoclave synthesized MnO$_2$/graphene composite as a cathode material for lithium–oxygen batteries. *J. Appl. Electrochem.* **2016**, *46* (8), 869–878.

(58) Wang, L.; Cui, X.; Gong, L.; Lyu, Z.; Zhou, Y.; Dong, W.; Liu, J.; Lai, M.; Huo, F.; Huang, W.; Lin, M.; Chen, W. Synthesis of porous CoMoO4 nanorods as a bifunctional cathode catalyst for a Li-O$_2$ battery and superior anode for a Li-ion battery. *Nanoscale* **2017**, *9* (11), 3898–3904.

(59) Gong, Y.; Ding, W.; Li, Z.; Su, R.; Zhang, X.; Wang, J.; Zhou, J.; Wang, Z.; Gao, Y.; Li, S.; Guan, P.; Wei, Z.; Sun, C. Inverse Spinel Cobalt–Iron Oxide and N-Doped Graphene Composite as an Efficient and Durable Bifunctional Catalyst for Li-O$_2$ Batteries. *ACS Catal.* **2018**, *8* (5), 4082–4090.

(60) Kim, J. G.; Noh, Y.; Kim, Y.; Lee, S.; Kim, W. B. Fabrication of three-dimensional ordered macroporous spinel CoFe$_2$O$_4$ as efficient bifunctional catalysts for the positive electrode of lithium–oxygen batteries. *Nanoscale* **2017**, *9* (16), 5119–5128.